Unraveling the role of support membrane chemistry and pore properties on the formation of thin-film composite polyamide membranes

Yu Jie Lim[a,b,c], Kunli Goh[a], Gwo Sung Lai[a], Yali Zhao[a], Jaume Torres[a,d], Rong Wang[a,b,*]

[a] Singapore Membrane Technology Center, Nanyang Environment and Water Research Institute, Nanyang Technological University, 637141, Singapore

[b] School of Civil and Environmental Engineering, Nanyang Technological University, 639798, Singapore

[c] Interdisciplinary Graduate Programme, Graduate College, Nanyang Technological University, 637553, Singapore

[d] School of Biological Sciences, Nanyang Technological University, 637551, Singapore

*Corresponding author. Singapore Membrane Technology Center, Nanyang Environment and Water Research Institute, Nanyang Technological University, 637141, Singapore

*E-MAIL: rwang@ntu.edu.sg (R. Wang)

Abstract

Nanoscale characteristics of the polyamide layer are key towards the high desalination performance of thin-film composite reverse osmosis (TFC-RO) membranes. Further advancements in the performance of TFC membranes necessitate a comprehensive understanding of the desired polyamide characteristics and its formation mechanisms. Empirical evidence has shown that the properties of the support layer is as equally important as the interfacial polymerization (IP) conditions in the fabrication of high permselectivity TFC membranes for desalination. Herein, we discuss the properties of polyamide layers formed using identical IP conditions over support membranes of different polymers and chemistries (polyethersulfone, polyetherimide and polysulfone) under fairly similar surface pore properties. The characteristics of the polyamide layers formed thereon displayed different physicochemical properties. It is postulated that the support membrane chemistry actually affects the IP reaction and polyamide formation by controlling the amine diffusion speed as well as the breadth of the IP reaction zone (*i.e.*, the region between the interface and the furthest point in which the reaction occurs). Transmission electron microscopy analyses further revealed the nanoscale differences in the polyamide layer (heights ranging from 50-200 nm), including intrinsic thickness of basal layer (~10-35 nm) and leaf-like top layer (~20-85 nm), as well as the presence of nanovoids. Finally, we propose a conceptual model to underline the role of support membrane chemistry in the IP reaction, and consequently the formation mechanism of the nanoscale polyamide features. The mechanistic insights from this study are expected to provide more understanding towards a better control over the fabrication of polyamide layers for TFC membranes. The findings in this work are also expected to facilitate tailoring polyamide layers for specific osmotically driven processes.

Keywords: Thin-film composite membrane; support membrane chemistry; polyethersulfone; polyetherimide; polysulfone; interfacial polymerization.

1. Introduction

The thin-film composite (TFC) membrane is currently the gold standard for the membrane desalination industry, with most of the reverse osmosis (RO)-based desalination plants worldwide adopting the commercial TFC membranes for seawater desalination and water purification [1, 2]. Ever since its inception about 50 years ago, this type of membrane has not changed much in terms of its fundamental design and concept. The TFC membrane consists of three main components: 1) a polyester non-woven fabric for bulk mechanical strength, 2) a microporous polymeric substrate as support layer, and 3) an ultrathin but dense polyamide thin-film as selective layer capable of separating solutes and water [1, 3]. In a typical RO separation process, pressure is applied onto the feed side of the membrane to enable selective transport of water over solutes through the polyamide layer.

The polyamide layer of RO membranes is typically formed *in situ* on the top side of the microporous support *via* interfacial polymerization (IP) (Fig. 1A). The fundamental mechanism of IP is based on the Schotten-Baumann reaction, in which an extremely fast and irreversible reaction occurs immediately when two different monomers come into contact, typically between a diamine and acyl chloride dissolved in aqueous and organic phase, respectively [4, 5]. The immiscible nature of the two phases (*i.e.*, water and oil) will restrict the reaction to only occur near the phase boundary. Because of the slightly higher solubility of amines in the organic phase as compared to acyl chlorides in the aqueous phase, the reaction occurs predominantly at the organic phase adjacent to the phase boundary [6]. At the initial stage of IP, m-phenylenediamine (MPD) will diffuse into the organic phase to react with trimesoyl chloride (TMC), forming a nascent basal polyamide layer that is approximately 20-50 nm in thickness [7, 8] (Figs. 1B and 1C). Thereafter, MPD will continue to diffuse through the basal polyamide layer (into the organic phase) to react with TMC, forming random

polyamide leaves (thickness of ~20-100 nm) stacked on top of the basal layer, which is manifested by the ridge and valley protuberances in the polyamide layer of RO membranes (overall heights ranging from 100 to 300 nm) [1, 9, 10]. The IP reaction will self-terminate when amine monomers cannot diffuse further into the organic phase due to the resistance posed by the polyamide layer.

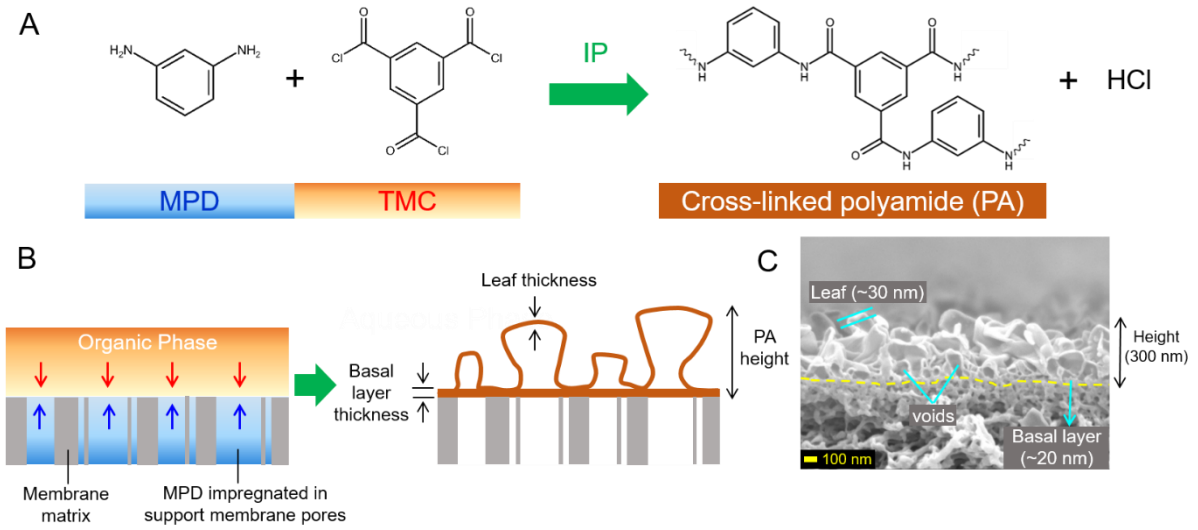

Fig. 1. (A) The IP reaction between MPD and TMC to form a cross-linked polyamide. **(B)** Schematic illustration of the eventual polyamide film formed in IP. The polyamide height, basal layer thickness and leaf thickness are illustrated. **(C)** Cross-sectional scanning electron microscopy (SEM) image of the polyamide layer of a commercial RO membrane (Hydranautics ESPA2-4040). The yellow dotted line depicts the boundary between the support layer and selective layer.

Because of the ultrathin and heterogeneous (i.e. internal structure variation) nature of the polyamide layer, it is challenging to determine which aspects of the polyamide affect the performance of desalination membranes to the greatest extent. For example, general consensus suggests that the polyamide layer should be thin (*i.e.*, low heights) to minimize the resistance to the diffusion of water but sufficiently dense to ensure the selective transport of water over solutes (*i.e.*, to obtain high permeability and selectivity, respectively) [1]. However, another study showed that the homogeneity in local polyamide density holds the key to maximizing membrane permselectivity even if the polyamide layers are of greater heights [11]. Regardless

of the reasons, it is clear that fine-tuning of the nanoscale polyamide characteristics is crucial to improving the permselectivity of TFC membranes, which is the reason why many studies have attempted to comprehensively understand the formation mechanism of the polyamide layers *via* IP. However, the extremely fast and complex nature of IP makes it difficult to observe the detailed IP mechanism. To date, certain features of the polyamide film and its formation mechanisms are still not completely understood, as evidenced by the diverse proposed mechanisms in the literature [1, 6, 12], which were mostly hypothesized based on the characteristics of the eventual polyamide layers obtained after the IP reaction.

To fabricate membranes with high permselectivity, most research works focused on fine-tuning the properties of the polyamide layer *via* the optimization of IP conditions (*e.g.* choice of monomers, additives, curing conditions) [13-15]. However, it must be acknowledged that the properties of the support membrane are as important as the IP conditions, considering that it affects the interface between the two phases and eventually the formation mechanism of the polyamide selective layer. The crucial parameters of the support membrane include the pore properties (pore size, porosity, roughness and pore distributions) and its surface chemistry [7, 16, 17], whereby they control the diffusion speed and extent of MPD partitioning into the organic phase, which ultimately affects the nanoscale structure of the polyamide layer and its separation performance.

In this work, we rationally study the effect of support membrane chemistry on the polyamide formation mechanism using three types of support materials: polyethersulfone (PES), polyetherimide (PEI) and polysulfone (PSf). These three types of materials have been commonly used as support membranes for a wide range of osmotically driven applications, including forward osmosis and pressure retarded osmosis [18, 19]. This work provides a

systematic understanding of the role of support material chemistries in the fabrication of TFC membranes for RO application. It is postulated that the support membrane chemistry (under fairly similar surface pore characteristics) affects the extent of polymerization by controlling the MPD diffusion speed and the breadth of the IP reaction zone (*i.e.,* the region between the interface and the furthest point in which the reaction occurs) which eventually dictates the nanoscale characteristics of the polyamide layer. From the findings in this study, we propose a conceptual model describing the role of support membrane chemistry in controlling the morphology of the polyamide layer, and affecting the desalination performance of TFC-RO membranes.

2. Experimental

2.1 Materials and chemicals

Unless otherwise stated, all chemicals are of reagent grade and were purchased from Sigma-Aldrich, USA. The chemicals were used directly without any further modification or purification. 1-Methyl-2-pyrrolidinone (NMP) and Dimethylformamide (DMF) were used as organic solvents to dissolve polymeric resins in the preparation of dope solutions. The three types of polymeric resins used were Polyethersulfone (PES, Ultrason E 6020 P, BASF, Germany), Polyetherimide (PEI, Ultem 1000, SABIC, Saudi Arabia) and Polysulfone (PSf, Udel P-3500, Solvay, Belgium). Deionized (DI) water (Milli-Q ultrapure grade) was used in the preparation of aqueous solutions. m-Phenylenediamine (MPD) flakes and Trimesoyl chloride (TMC, liquid form) were used to synthesize the polyamide selective layer *via* interfacial polymerization (IP). N-hexane (>99% purity) was used as the organic solvent to dissolve liquid TMC. Dimethyl sulfoxide (DMSO) and Triethylamine-Camphorsulfonic acid (TEA-CSA) salt were used as additives in the aqueous phase of IP.

2.2 Preparation and characterization of the polymer solutions

A total of six polymeric dope solutions (Table 1) were prepared in this study using NMP and DMF as organic solvents. The 10 wt% and 16 wt% polymeric dope solutions were used to fabricate the low concentration (LC) and high concentration (HC) support membranes, respectively. The polymer solutions were made from different solvent compositions (Table 1) to control the solvent and non-solvent exchange rates in the phase separation process [20, 21], so as to facilitate the fabrication of support membranes with expected surface pore properties. The dope solutions were stirred and dissolved overnight with mild heating at 60 ^{o}C to ensure full dissolution of the polymeric resins. The specific compositions and viscosities of the dope solutions are outlined in Table 1, with the latter measured using a rheometer (Physica MCR 301, Anton Paar, Austria) at a shear rate of 10 s^{-1} under 25 ^{o}C.

Table 1. The compositions and viscosities of polymeric dope solutions used in the fabrication of the support membranes. The support membranes were prepared based on low concentration (10 wt% polymer) and high concentration (16 wt% polymer) polymer dope solutions.

Support membrane	Dope composition		
	Polymer concentration (wt%)	Solvent composition (Ratio of NMP:DMF)	Viscosity (mPa·s)
PES-LC	10	1:0	106.8 ± 2.7
PEI-LC	10	4:11	39.2 ± 1.3
PSf-LC	10	1:7	51.1 ± 0.1
PES-HC	16	1:0	627.5 ± 3.8
PEI-HC	16	4:11	360.9 ± 9.5
PSf-HC	16	1:7	760.5 ± 21.3

2.3 Fabrication of the support membranes

The microporous support membranes were fabricated by a non-solvent induced phase inversion method (NIPS) according to our previous works [20]. Prior to the casting process, the dope solutions were cooled down to room temperature and degassed under vacuum for 10 min to remove any bubbles present in the solutions. First, a piece of nonwoven fabric

(E055094-74, MIKI & CO., LTD., Japan) was fixed onto a dry glass plate using laboratory adhesive tape. To prevent the dope solution from penetrating into the non-woven fabric, the latter was pre-wetted with the respective solvents (Table 1) prior to the casting process [22]. Next, a micrometer film applicator (Elcometer 3530, UK) was used to uniformly spread the casting solution on the nonwoven fabric. The gate height of the film applicator was set to 200 µm. After 2 s delay time, the glass plate was then immersed into the coagulant bath (tap water at 24.5 ^{o}C) to form the support membranes. The nascent support membranes were washed thoroughly with MQ water and transferred into a MQ water container after 20 min of stabilization time and soaked overnight prior to IP.

2.4 Fabrication of the TFC membranes *via* interfacial polymerization

The polyamide selective layer was fabricated on top of the support membrane *via* an IP reaction between MPD and TMC. In brief, three types of solutions were employed in the IP process: 2% (w/v) MPD aqueous solution, 0.1% (w/v) TMC solution dissolved in hexane, and pure hexane. 1% (w/v) DMSO as well as TEA-CSA salt were added into the MPD solution as flux-enhancing additives to catalyze the IP reaction, as per reported previously [23]. To isolate the influence of the support membrane properties in affecting the polyamide properties, the same IP formula was used in the fabrication of all TFC membranes. The TFC membranes synthesized using LC supports were labeled as TFC-PES-LC, TFC-PEI-LC and TFC-PSf-LC, whereas the TFC membranes synthesized using HC supports were named as TFC-PES-HC, TFC-PEI-HC and TFC-PSf-HC.

The same IP procedure was adopted as per reported in our previous works [23]. In brief, the support membranes were immersed in MPD aqueous solution for 1 min to ensure MPD impregnation into the pores of the support membranes. According to literature, 1 min of

immersion time should be sufficient to ensure complete MPD penetration into the surface pores [20], thereby ensuring the same extent of MPD impregnation for all support membranes in this work. Thereafter, excess MPD solution was purged off the support membrane surface using an air-knife. Next, the MPD-impregnated support membranes were contacted with TMC solution for 1 min to ensure complete reaction between MPD and TMC, before rinsing with pure hexane to wash off the excess TMC. Lastly, the membranes were thermally cured at a 60 ^{o}C forced convection oven for 10 min to induce further cross-linking of the selective layer.

2.5 Membrane characterization

Unless otherwise mentioned, the membrane samples were dried and kept in a desiccator for 32 h prior to characterization. Attenuated total reflection-fourier transform infrared spectroscopy (ATR-FTIR, Shimadzu, Japan) was used to detect the functional groups of the support and TFC membranes. The spectra from 400-4000 cm^{-1} were collected from the FTIR spectrometer with a sampler at a resolution of 4 cm^{-1}. In addition, the cross-linking degrees of the polyamide layers were determined using two methods: 1) the extent of the unreacted acyl chloride peak at ~945-955 cm^{-1} in FTIR analysis (obtained right after the curing process) and 2) the O/N and C/N ratios in X-ray photoelectron spectroscopy (XPS, AXIS Supra, UK), as per reported previously [23]. The scan area for XPS was 300 × 700 μm and the binding energy of the elements were calibrated based on the reference C1s peak at 285 eV.

The surface morphology and cross-sectional properties of the membranes were analyzed using field-emission scanning electron microscopy (FESEM, JEOL, Japan) at 5.0 kV. The samples were coated with a platinum layer for 100 s at 30 mA to make the membranes electrically conductive prior to FESEM analysis. The surface porosity and mean pore diameter

(μ_p) of the top surface of the support membranes were estimated using Image J software on FESEM images, as per described in previous studies [9, 24]. The surface pore size distribution of the support membranes were tabulated based on the following equation:

$$\frac{df(d_p)}{d(d_p)} = \frac{1}{d_p \ln \sigma_p \sqrt{2\pi}} \times \exp\left[-\frac{(\ln d_p - \ln \mu_p)^2}{2(\ln \sigma_p)^2}\right] \quad (1)$$

where d_p and σ_p are the pore diameter and geometric standard deviation, respectively [25]. To analyze the cross-sections of the membranes, the membranes were freeze fractured in liquid nitrogen after 5 min immersion time. The polyamide cross-sections of the TFC membranes were also analyzed using transmission electron microscopy (TEM, JEM-1400, JEOL, Japan) at an operating voltage of 120 kV. The samples were embedded in liquid LR White resin for 24 h prior to continuous curing at 60 °C for 72 h. The solidified resins were cut using a shaving blade to expose the membrane prior to sectioning by an ultramicrotome with an oscillating diamond knife. The eventual ~60-70 nm thick sections were then transferred to copper grids for TEM characterization.

The surface roughness of all membranes were investigated using an atomic force microscope (AFM, Park XE-100, Korea) equipped with an AFM probe (PPP-NCHR, Nanosensors™). The mean width of the cantilever is 30 μm with a tip radius of less than 7 nm. The membranes were fixed onto the specimen holder and 25-μm^2 areas were scanned in a non-contact mode, with the roughness quantified by a roughness average (R_a). The hydrophilicity of the membranes were determined by measuring the water contact angles, as per reported previously [23]. At least 10 equilibrium measurements were obtained for each membrane sample.

2.6 Membrane filtration tests

The TFC membranes were soaked in DI water for at least 10 h prior to the RO membrane tests. The performance of TFC-RO membranes were evaluated using a cross-flow filtration setup equipped with multiple permeation cells (CF042D-CF, Sterlitech, USA). The TFC membranes were secured in the cells with the polyamide layer facing the feed stream, and the active area of each membrane coupon is 42 cm^2. The RO cross-flow tests were conducted using 2000 ppm NaCl feed solution (neutral pH) at a hydraulic pressure of 15.5 bar (225 psi). The temperature of the feed tank was kept constant at 25.0 $\pm$ 0.2 ℃ by a recirculating chiller (XT5618B8, Xtemp Temptech, China). The crossflow velocity was maintained at ~0.15 m/s for all experimental runs. In order to minimize the influence of compaction factor on the membrane performance [23, 26], all TFC membranes were first pressurized at 15.5 bar using pure water for 1 h to stabilize the water flux. Thereafter, the membranes were pressurized for another 1 h using 2000 ppm NaCl feed solution before data collection.

The water flux (J_w) (L m^{-2} h^{-1}; LMH) was measured by a mass flow meter (mini CORI-FLOW™, Bronkhorst, Netherlands) and the salt rejection (R) was calculated based on the concentration difference between the feed (C_f) and permeate (C_p) measured using a digital conductivity sensor (UniCond, Mettler Toledo, Ohio, USA):

$$R = 1 - C_p/C_f \qquad (2)$$

The water and inverse salt permeability coefficients (denoted as A and $1/B$ respectively) of the TFC membranes were tabulated as follows:

$$A = \frac{J_w}{(\Delta P - \Delta \pi)} \qquad (3)$$

$$\frac{1}{B} = \frac{1}{J_w} \times \left(\frac{R}{1-R}\right) \qquad (4)$$

where ΔP and $\Delta\pi$ corresponds to the applied hydraulic pressure (15.5 bar) and the osmotic pressure difference (~1.57 bar according to [1]) across the semi-permeable membrane.

3. Results and discussion

3.1 Characteristics of the support membranes

3.1.1 Chemical properties

The chemical characteristics of the three support membranes were differentiated based on the functional groups present in the chemical structures. First, the PEI support membranes showed bands at ~1778 cm^{-1} and 1723 cm^{-1} (Fig. 2), which are characteristic of the unique asymmetric and symmetric stretching of the C=O bonds (imide I) [27, 28]. In addition, the distinctive bands at ~1600 cm^{-1} and ~1357 cm^{-1} are the representative of the stretching of the C-N bonds in imide II [27, 29]. For PES and PSf membranes, the FTIR spectra showed broad bands at ~1585 cm^{-1}, 1487 cm^{-1} and 1325 cm^{-1} (Fig. 2). The former two are attributed to the presence of the benzene rings [30] whereas the latter is the representative of the S=O bonds. It is noticed that two additional minor bands at ~1386 cm^{-1} and 1366 cm^{-1} were present in PSf support, which are attributed to the unique presence of the methyl groups in PSf (Fig. 2) [30]. It is also noticed that there were no minor bands at 1386 cm^{-1} and 1366 cm^{-1} for the PEI supports (despite the presence of methyl groups), which is plausible given that the intense band at ~1357 cm^{-1} likely suppressed any minor bands in the range of ~1400-1320 cm^{-1} [28].

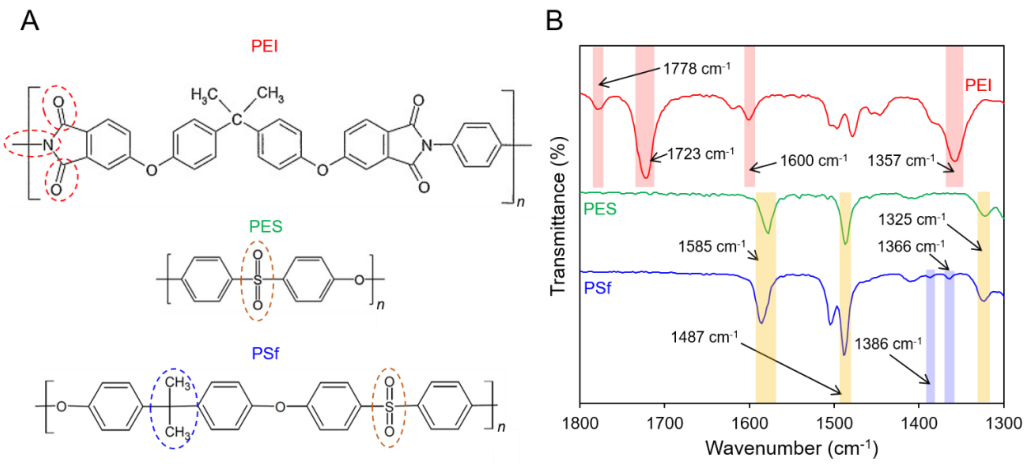

Fig. 2. (A) Chemical structures of the three polymers used in the fabrication of support membranes. The red dotted circles outline the unique bonds present in polyetherimide (PEI) whereas the brown dotted circles outline the common S=O bond present in polyethersulfone (PES) and polysulfone (PSf). The blue dotted circle representing the methyl groups in PSf can be used to distinguish PSf from PES. **(B)** FTIR spectra outlining the representative chemical bonds which can be used to distinguish the three support membranes.

3.1.2 Surface properties

The surface FESEM images of the support membranes are presented in Fig. 3. First, it is noticed that the LC support membranes have a higher surface porosity as well as larger surface pores when compared against the HC support membranes. Quantitative analysis revealed that the LC support membranes have surface porosities of ~8-11%, with average pore sizes ranging from 22-28 nm (Fig. 4). On the other hand, the HC support membranes have low surface porosities of ~2-4% and pore sizes of ~13-19 nm (Fig. 4). The more porous surfaces of the LC support membranes can be attributed to the much lower viscosity of the dope solutions of LC as compared to HC (Table 1). Notably, the LC membranes were fabricated from dope solutions with viscosities of ~50−100 mPa·s, which is much lower than that of HC membranes fabricated from dope solutions with viscosities of ~400−800 mPa·s. The much lower viscosity of the LC dope solutions probably allow the non-solvent (water) to penetrate and diffuse into the polymer solution more rapidly during the initial stage of the phase inversion process, which consequently resulted in the formation of support membranes with more porous surfaces [20,

24, 31]. Apart from that, the PEI, PES and PSf membranes have fairly similar surface pore properties when compared within their LC and HC levels.

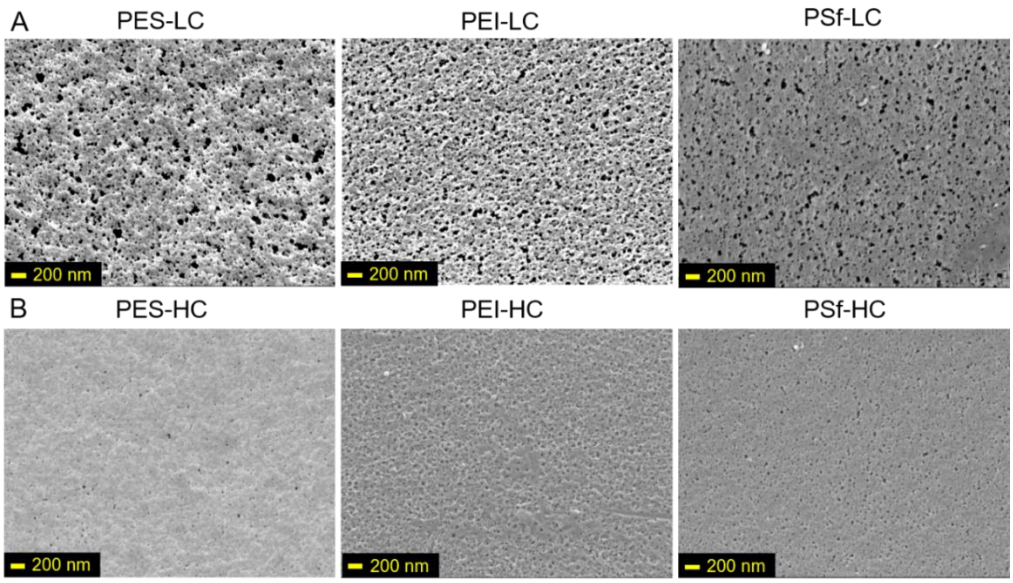

Fig. 3. Surface FESEM images of the **(A)** low concentration (LC) support membranes and **(B)** high concentration (HC) support membranes in this work. LC and HC membranes were made from the dope solution consisting of 10 wt% polymer and 16 wt% polymer, respectively.

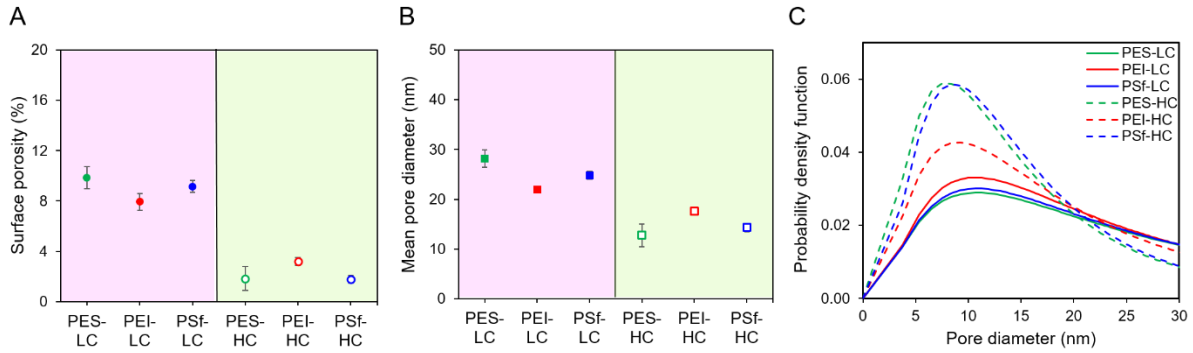

Fig. 4. Surface pore properties of the LC and HC support membranes. **(A)** Surface porosity. **(B)** Mean pore diameter (nm). **(C)** Surface pore size distribution (PSD). The PSD is a mathematical function that defines the relative amount of pores present according to the pore diameter, whereas the mean pore diameter is the average pore size obtained from image analysis. Error bars are standard deviations based on three independent samples.

The much more porous surfaces of the LC membranes were also supported by the roughness measurements (R_a ~ 15-17 nm), when compared against the HC membranes (R_a ~ 9-12 nm) (Fig. 5A). This observation is plausible given that more porous surfaces typically exhibit higher roughness values [8, 32], due to the greater presence of surface apertures

recorded by the probe during AFM scans. Contact angle analyses in Fig. 5B revealed that the support membranes showed distinctly different levels of wettability with hydrophilicity decreases in the order of PES > PEI > PSf (trend is valid for both LC and HC supports), which is consistent with the literature [30].

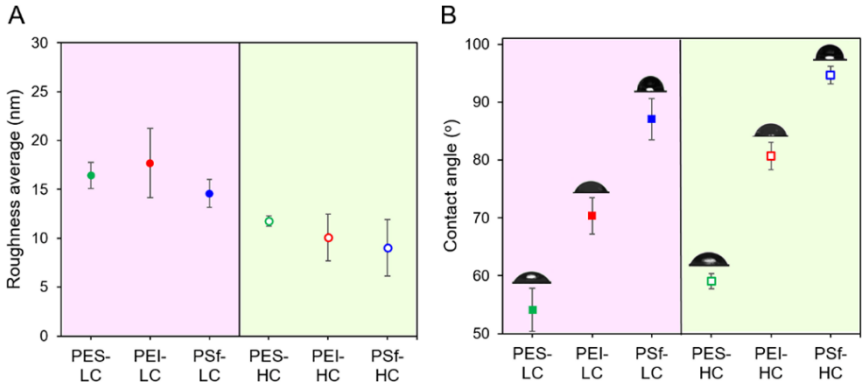

Fig. 5. Surface properties of the LC and HC support membranes in terms of the roughness average **(A)** and hydrophilicity using contact angle analysis **(B).** A static contact angle image is presented together with the respective contact angle in (B). Error bars are standard deviations based on three independent samples.

3.1.3 Cross-sectional properties

According to the FESEM cross-sectional images in Fig. 6, it is noticed that the six support membranes possessed distinctly different sublayer structures. The variation in the sublayer structures is intrinsically controlled by the demixing process which is dependent on the combination of thermodynamic and kinetic factors of the phase separation process. The former is determined by the affinity between the polymer and solvent mixture whereas the latter is dependent on the dope viscosity [20, 21, 32]. According to Table 2, the solubility parameter difference between the polymer and the solvent mixture is in the order of PSf > PEI > PES. A higher solubility parameter difference means that the polymer solution is more thermodynamically unstable (*i.e.,* the solvent mixture is less compatible with the polymer) [20]. Hence, it can be concluded that the thermodynamic stability of the polymer solution increases in the order of PSf < PEI < PES.

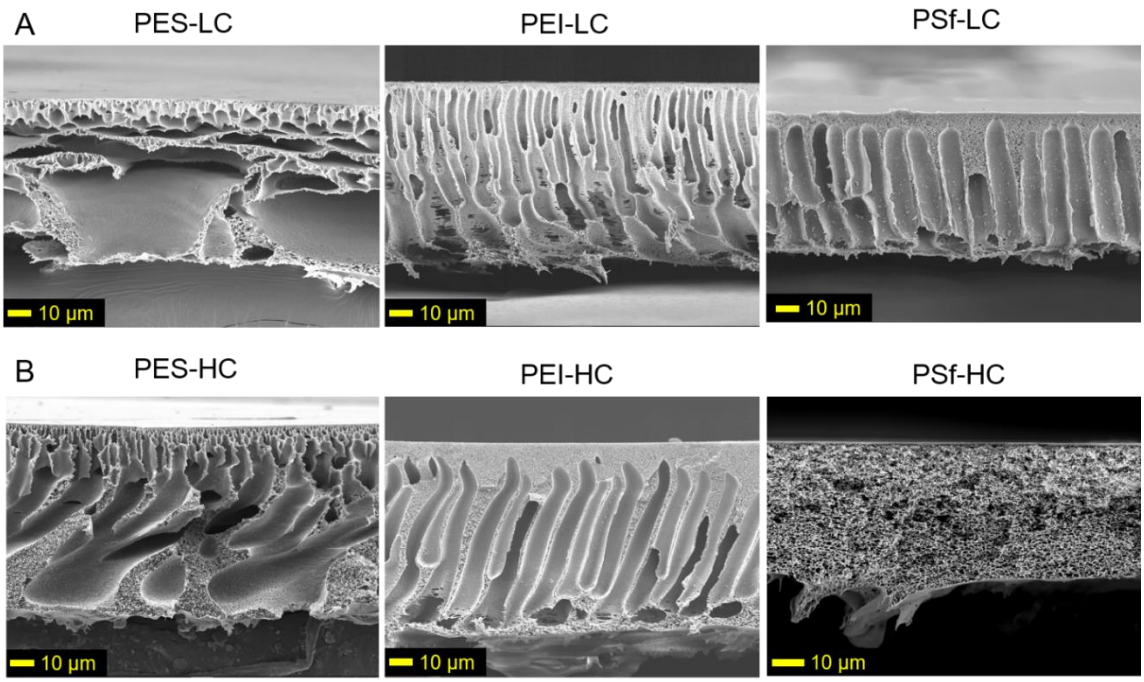

Fig. 6. Cross-sectional FESEM images of the **(A)** low concentration (LC) support membranes and **(B)** high concentration (HC) support membranes in this work. LC and HC membranes were made from the dope solutions consisting of 10 wt% polymer and 16 wt% polymer, respectively.

Table 2. Hansen solubility parameters (δ_{sp}) of polymeric dope solutions used in this study. The difference in solubility parameters were used to estimate the thermodynamic stability of the dope solutions. The solubility parameters were calculated based on the literature [33].

Dope solution	Hansen solubility parameter ($MPa^{1/2}$)		
	δ_{sp} (polymer)	δ_{sp} (solvent)	$\lvert\delta_{sp}\ (\text{polymer}) - \delta_{sp}\ (\text{solvent})\rvert$
PES-LC/ -HC	24.19	22.96	1.23
PEI-LC/ -HC	22.87	24.35	1.48
PSf-LC/ -HC	22.93	24.62	1.69

First, the thermodynamically unstable PSf-LC dope likely predisposed the polymer solution to undergo gelation at the initial stage (due to large solvent outflow), which led to the formation of a homogeneous sponge-like skin layer (~5 µm) [21, 34]. Next, it is hypothesized that the nascent sponge-like skin layer facilitated the uniform penetration of the non-solvent in a controlled fashion, which is manifested by the straight macrovoids in the sublayer [20]. As for the PSf-HC membrane, the same concept can be used to explain the formation of the sponge-like skin layer except that the subsequent advancement of the polymer-lean phase was

hindered due to the high viscosity of the dope solution [35]. This subsequently resulted in the formation of a sponge-like structure throughout the remaining of the sublayer [36, 37].

As compared to the PSf dope solutions, the more thermodynamically stable nature of the PEI dope solutions (Table 2) resulted in a lower extent of initial gelation for PEI-LC, as represented by the thinner sponge-like skin layer (~2 μm) [37, 38]. Thereafter, some of the initial polymer-lean phase might have merged and moved forward in the process, resulting in the formation of slightly bigger macrovoids at the bottom of the sublayer [20]. As for the PEI-HC membrane, the much higher viscosity relative to PEI-LC probably resulted in the delayed penetration of the non-solvent, thereby forming a thicker sponge-like skin layer (~10 μm) [37, 38]. The thick sponge-like skin layer likely encouraged the orderly advancement of the polymer-lean phase, which is manifested by the columnar macrovoids underneath [20].

The thermodynamically stable nature of the PES dope solutions (Table 2) is known to result in slow initial demixing whereby liquid-liquid demixing occurs before the gelation process [20, 21]. This creates a polymer-rich and polymer-lean phases corresponding to the membrane matrix and pores respectively, which is exhibited by the skin layer comprising tiny macrovoids. Subsequently, some of the advancing polymer-lean phase could have merged and advanced forward in a disorderly fashion, which is evidenced by the transition of small macrovoids at the skin layer into bigger and irregularly-shaped macrovoids at the bottom of the sublayer [37, 39].

359 ### 3.2 Characteristics of the selective layers

360 #### 3.2.1 Physical characteristics of the selective layers

361 Given that identical IP formulas were used to fabricate the TFC membranes, the
362 changes in the properties of the polyamide layers can only be attributed to the support
363 membrane chemistry (under similar pore properties) or pore structure (under a similar support
364 membrane material). First, it is noticed from the surface FESEM images that the TFC-PES and
365 TFC-PSf membranes (Figs. 7A/B and 7E/F, respectively) have the 'ridge and valley' type
366 morphologies that is characteristic of the polyamide nodules formed using the MPD-TMC
367 chemistry [1]. However, the TFC-PEI membranes (Figs. 7C/D) showed different surface
368 morphologies in that the polyamide nodules seems to be connected and interlinked, thereby
369 forming polyamide sheets comprising clumpy roof-like surfaces. Cross-sectional TEM
370 analyses (Fig. 7) revealed that the heights of the polyamide layers decrease in the order of TFC-
371 PSf > TFC-PEI > TFC-PES, with this trend being valid for both TFC membranes made from
372 LC and HC supports.

373

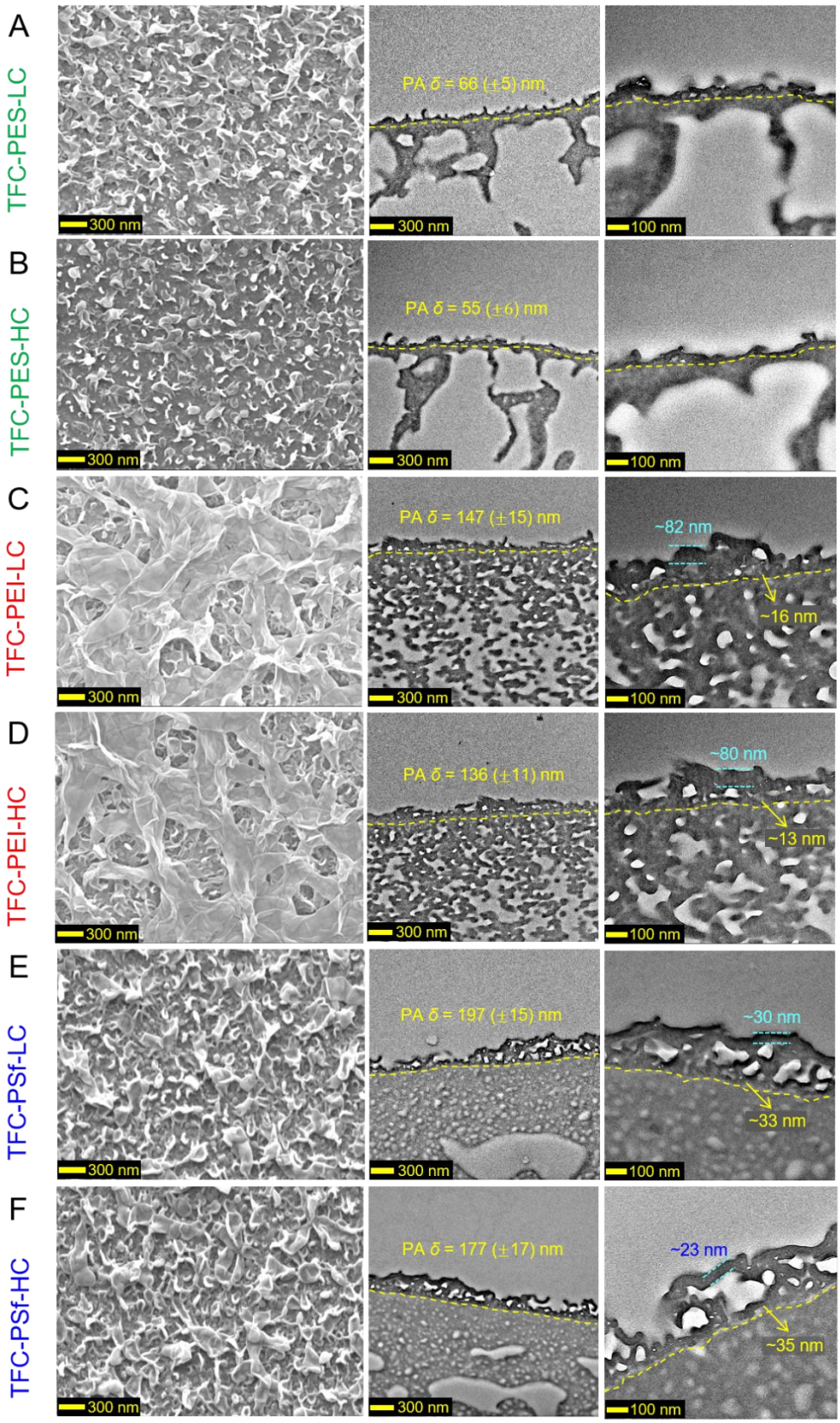

Fig. 7. The surface and cross-sectional properties of the polyamide layers of the TFC membranes. **Leftmost images:** Polyamide surface morphology in SEM images. **Middle images:** Polyamide selective layer height (δ) from cross-sectional TEM images. The yellow dotted line denote the boundary between the polyamide and support layer. **Rightmost images:** High magnification TEM images outlining the cross-section of the polyamide layers.

It is observed that the TFC-PES membranes comprise an ultrathin polyamide layer (heights of ~50-70 nm) without nanovoids (Figs. 7A/B), which we attribute to the hydrophilic nature of the PES support membranes (see Fig. 5B). A hydrophilic support membrane is known to reduce MPD diffusion speed as well as the extent of partitioning into the organic phase during IP because of the affinity between the support and the MPD aqueous solution [40]. The much slower MPD diffusion and less vigorous IP reaction likely quenched the formation of nanovoids during the exothermic reaction, as seen by absence of nanovoids in the polyamide layers of TFC-PES membranes [41]. The high affinity between MPD and the support membrane will not only result in a lower extent of partitioning into the organic phase, but also constrict the IP reaction to occur inside the pores of the support such that some of the polyamide might sag into the pores of the support [40, 42, 43]. Overall, this led to the formation of polyamide layers with low apparent heights and minimal protuberances (*i.e.*, manifested by the less evident polyamide leaves) [42], whereby the latter is also reflected in the relatively smoother surfaces of the TFC-PES membranes when compared against TFC-PEI and TFC-PSf membranes (Fig. 8).

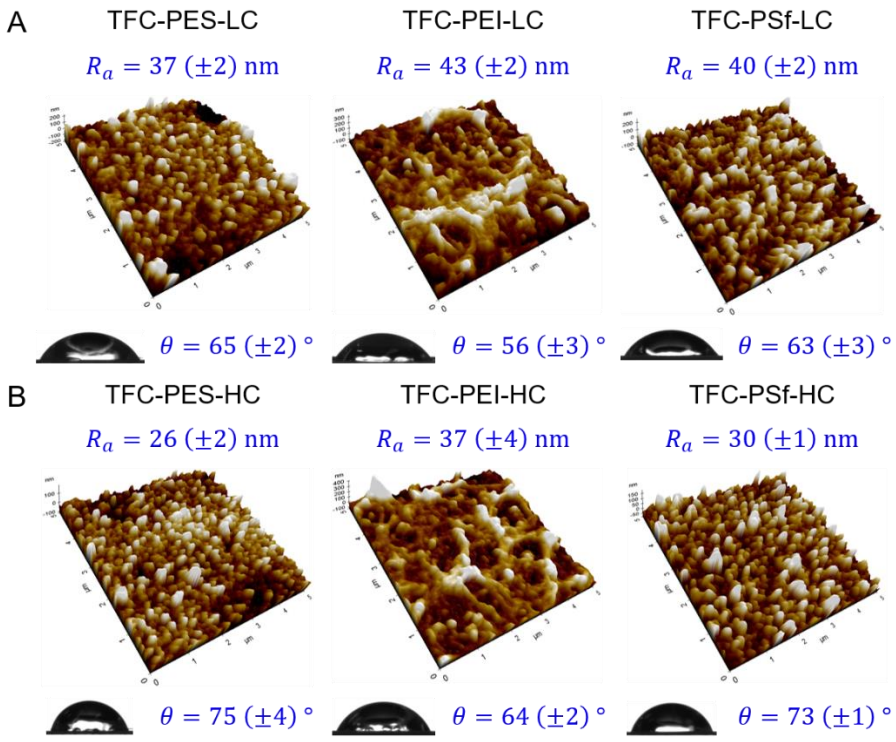

Fig. 8. Surface properties of the **(A)** TFC-LC and **(B)** TFC-HC membranes presented in terms of the roughness average (R_a) and hydrophilicity using contact angle analysis. The individual 3D images in AFM and static contact angle images of the TFC membranes are presented for visualization purposes. Error bars are standard deviations based on three independent samples.

It is noticed that the polyamide layers of the TFC-PSf membranes (Figs. 7E/F) consist of a bit more nanovoids when compared to the TFC-PEI membranes (Figs. 7C/D). High magnification TEM analyses further revealed the differences in the polyamide layers at the nanoscale. First, the polyamide layers of the TFC-PSf membranes comprise a slightly thicker basal layer (~ 35 nm) with thinner polyamide leaves (~20-30 nm), and there were multiple nanovoids sandwiched in between these two layers. Conversely, the polyamide layers of the TFC-PEI membranes have a thinner basal layer (~ 15 nm) underneath thicker polyamide leaves (~ 80 nm), with much less nanovoids when compared against the TFC-PSf membranes. It is postulated that the more hydrophobic nature of the PSf supports encouraged the faster and greater extent of MPD monomer diffusion during IP. At the incipient stage, the fast vertical and lateral diffusion of MPD monomers led to the formation of a thick basal layer (~35 nm). Simultaneously, MPD monomers can diffuse further into the organic phase thereby forming

polyamide layers with greater heights [44]. The greater extent of MPD diffusion also means that the MPD monomers were more spread out over a larger breadth zone in the IP reaction, resulting in the formation of thinner polyamide leaves due to smaller amount of MPD monomers (to react with TMC) at any certain spot. The more vigorous MPD diffusion (*i.e.*, faster reaction kinetics) can also promote more intense vaporization of hexane as well as heat-induced turbulence during the exothermic IP reaction [44, 45], thereby forming more nanovoids in the polyamide layers (Figs. 7E/F).

Conversely, the less hydrophobic nature of the PEI supports (compared against the PSf supports) will ensue a slower and lesser extent of MPD monomer diffusion during IP. The former resulted in the formation of a thinner basal layer at the initial stage of IP [8], whereas the latter will mean the MPD monomers are more concentrated in a narrower reaction zone, thereby forming thicker polyamide leaves which can subsequently stack and aggregate to form clumpy roof-like surfaces [7, 43] (Figs. 7C/D). The clumpy roof-like surfaces of the TFC-PEI membranes possibly explain its slightly rougher surface than the TFC-PSf membranes (when compared at the LC and HC scales), as evidenced in Fig. 8. Overall, the roughness and hydrophilicity trends of the TFC membranes (within the LC and HC levels) in Fig. 8 is noticed to decrease in this order: TFC-PEI > TFC-PSf > TFC-PES. The observed trend is in agreement with the Cassie-Baxter model since the surface roughness is known to enhance hydrophilicity of TFC membranes (for contact angles below 90º) [46].

3.2.2 Chemical characteristics of the active layers

As compared to the support membranes (Fig. 2B), the FTIR spectra of the TFC membranes (Fig. 9A) showed two additional bands at ~1663 cm^{-1} and 1538 cm^{-1}, which are characteristic of the amide I (*i.e.*, C=O stretching) and amide II (*i.e.*, N-H bending) bonds,

respectively, thereby confirming the successful fabrication of polyamide layers [8, 47]. It is also noticed that the TFC membranes made from LC and HC supports (under identical support material) showed similar peak intensities, suggesting fairly similar polyamide layer formation. The cross-linking degrees of the polyamide layers were further studied *via* narrow FTIR scans and XPS analyses. It can be inferred from Fig. 9B that the polyamide layers of the TFC-PEI membranes are less cross-linked than the TFC-PES/TFC-PSf membranes, as evidenced by the higher intensity of the unreacted acyl chloride peak at ~950 cm^{-1} [6, 23].

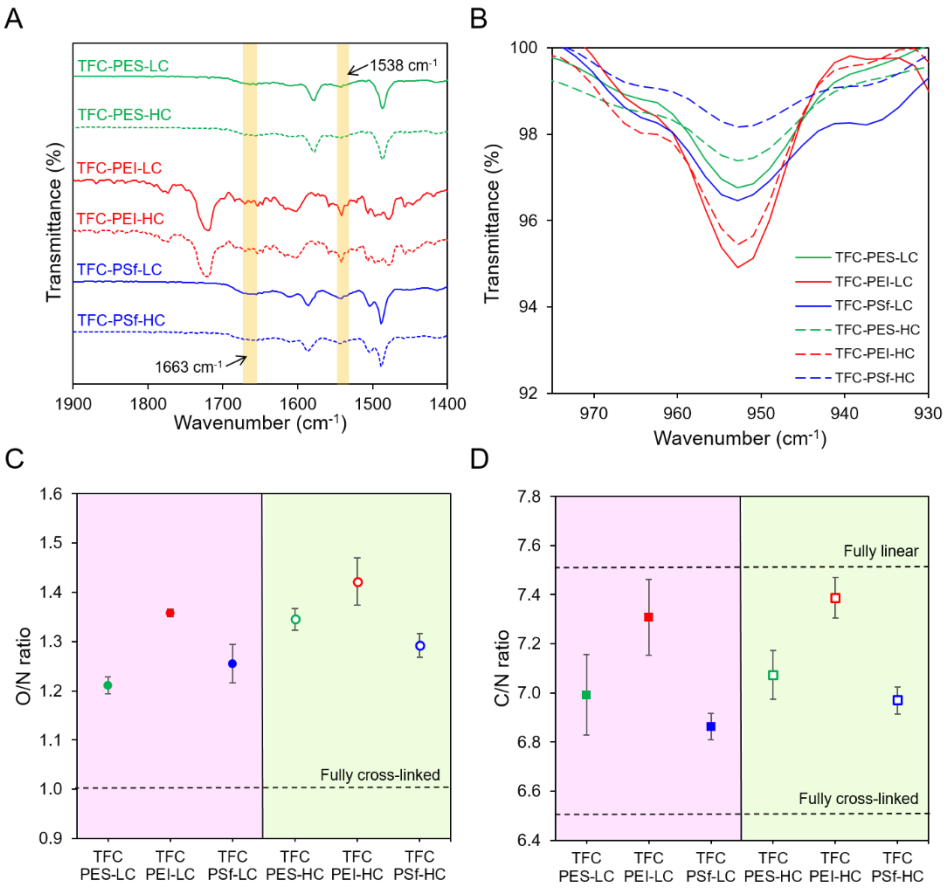

Fig. 9. (A) FTIR spectra of the TFC membranes. **(B)** FTIR analysis from 930-975 cm^{-1} that was obtained right after the membrane curing process. The amount of the unreacted acyl chlorides in the TFC membranes were estimated based on the intensity of the peak at 945-955 cm^{-1}. The cross-linking degrees of the polyamide layers were estimated based on the O/N **(C)** and C/N ratios **(D)** in XPS analyses.

This observation is further supported by the O/N and C/N ratio analyses in XPS (Figs. 9C and D). Theoretically, a fully cross-linked and fully linear polyamide have a molecular unit

of $C_{18}H_{12}N_3O_3$ and $C_{15}H_{10}N_2O_4$, respectively. This means that the theoretical O/N and C/N ratio ranges from 1-2 and 6-7.5, respectively, whereby a lower O/N and C/N ratio suggests the existence of a more cross-linked polyamide [48]. According to Figs. 9C and 9D, it is observed that the TFC-PEI membranes have a higher O/N and C/N ratio, indicating that the top polyamide layer is less cross-linked. Given the fact that XPS probes the top 5-10 nm of the polyamide layer, this observation is plausible because of the presence of the thick polyamide crumples of the TFC-PEI membranes (see section 3.2.1). According to literature, thick polyamide films are typically less dense assuming that the same amount of cross-linked polyamide is formed relative to thinner films [49].

3.3 Desalination performances of the TFC membranes

Fig. 10A presents the desalination performances of the TFC membranes in this work. Overall, the TFC membranes were able to achieve decent NaCl rejections of ~97.2−98.8%. For the TFC membranes made from LC or HC supports, it is observed that the water permeability decreases in the order of TFC-PEI > TFC-PSf >> TFC-PES. First, the low permeabilities of the TFC-PES membranes are likely attributed to the possibility that much of its polyamide layer sags into the pores of the support membranes (see Section 3.2.1). Empirical evidence from the literature suggests that the resistance for water diffusion through the selective layer will be dramatically increased if polyamide penetrates into the pores of the support layer [40, 43]. Thus, it is plausible that the water fluxes of the TFC-PES membranes are the lowest because of the greatest resistance for water diffusion through the selective layer, as compared to TFC-PEI and TFC-PSf membranes.

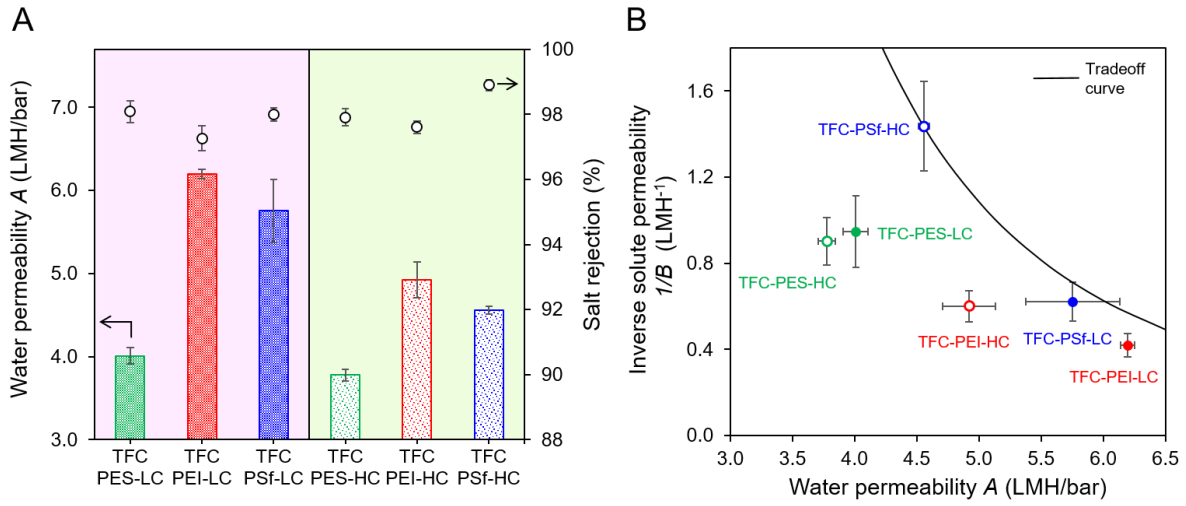

Fig. 10. (A) Water permeability and salt rejection of the TFC membranes prepared in this study. The IP formulas were identical in the fabrication of all TFC membranes. **(B)** The plot of inverse solute permeability (*1/B*) against water permeability (*A*) of the TFC membranes prepared in this study. The desalination performances were obtained at an operating pressure of 15.5 bar, using 2000 mg/L NaCl as feed solution. The equation for the tradeoff curve is: $1/B = 136.35A^{-3}$ (*i.e.*, $B \propto A^{3}$). Error bars are standard deviations based on three independent samples.

Next, it is noticed that the TFC-PEI membranes showed almost comparable permeability (only ~7% higher) as compared to TFC-PSf membranes (for both TFC membranes made from LC and HC supports). According to literature, the resistance posed by the polyamide layer to the diffusion of water molecules during RO operation is dependent on the overall mass transfer resistance posed by the polyamide leaves and the basal layer [41]. In this case, it can be argued that the resistance posed by much thicker polyamide basal layer of TFC-PSf membrane is offset by the much thinner polyamide leaves (see Section 3.2.1), thereby allowing the TFC-PSf membranes to attain fairly similar water permeability as compared to the TFC-PEI membranes. In addition, the slightly lower cross-linking degree of the TFC-PEI membranes (see Section 3.2.2) could have also contributed to the flux enhancement with respect to TFC-PSf membranes. It is also observed that the TFC-LC membranes generally showed higher permeability than the TFC-HC membranes (under a similar support membrane material), which is likely attributed to the more porous surface structure of the former. A more porous support membrane is known to reduce the resistance for water diffusion over the

selective layer during RO operation, thereby enhancing the water flux [20, 46]. From a permselectivity perspective, the TFC-PSf membranes demonstrated the best performance since it lies closest to the permselectivity tradeoff curve (Fig. 10B) [1]. This is especially true for the TFC-PSf-HC membrane with the highest *1/B* values at a decent permeability of ~4.6 LMH/bar (Fig. 10B), most likely attributed to the combination of the optimal polyamide characteristics (especially in terms of the cross-linking degree) and support properties (in terms of providing the most favorable support layer chemistry and pore properties for selective layer formation) that enabled its robust performance under RO conditions.

3.4 Proposed conceptual model for the impact of support membrane chemistry and pore properties in IP

Based on the results summarized in Sections 3.2 and 3.3, we propose a conceptual model depicting the potential impacts of the support membrane chemistry in affecting the IP mechanism and eventual polyamide characteristics (Fig. 11). For all TFC membranes fabricated in this study, the support membrane was first contacted with the MPD solution. After the air knife was applied to remove the excess MPD solution, it is likely that the MPD solution meniscus drops below the support interface for hydrophilic pores (*i.e.,* PES membranes) due to better wetting force, as per postulated by existing conceptual models [7, 40]. Furthermore, the affinity between the hydrophilic pore and MPD solution likely slowed down the MPD diffusion speed and extent (into the organic phase), thereby forming smooth polyamide layers with very low heights. The undersupply of MPD solution might lead to the formation of some polyamide inside the support membrane pores (Fig. 11), which explains the low permeability of TFC-PES membranes because of the increased resistance to water diffusion during RO operation.

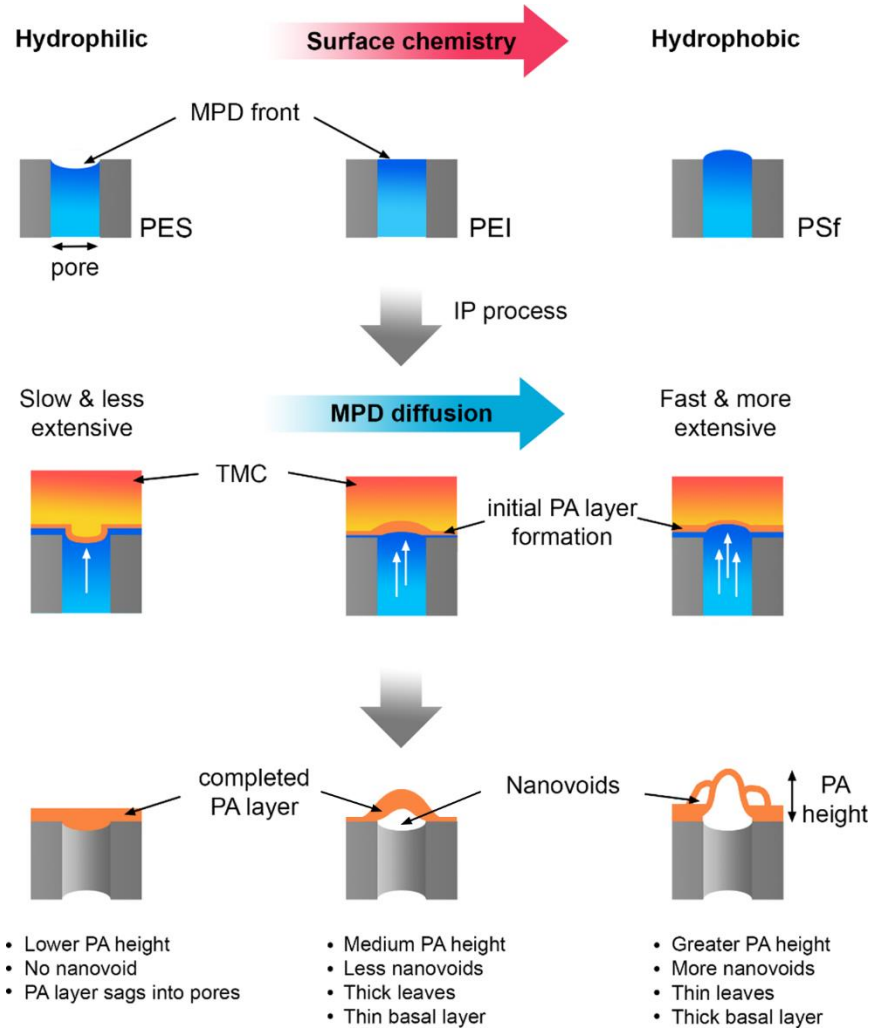

Fig. 11. Proposed conceptual model illustrating the role of support membrane chemistry in affecting the state of MPD meniscus after the air knife stage, the speed and extent of MPD diffusion into the organic phase and the eventual polyamide (PA) film properties.

For the other extreme end (*i.e.*, the most hydrophobic support: PSf), it is likely that the MPD solution meniscus protrudes above the hydrophobic support pores after the air knife stage because air de-wets the pores, as per hypothesized by a previous conceptual model [12]. Upon contact with TMC solution, the fast diffusion of MPD (lateral and vertical) results in the formation of a thick basal layer as well as a deeper diffusion into the organic phase (forming greater polyamide heights). However, this will mean that MPD monomers are more spread out over a larger breadth of the reaction zone, thereby forming thin polyamide leaves because of a lower local MPD concentration. As for the PEI support, which is less hydrophobic than PSf, the slightly slower and lesser extent of MPD diffusion likely resulted in the formation of a

thinner basal layer and polyamide layers with lower heights, respectively. However, the localization of MPD monomers over a narrower IP reaction zone will result in the formation of thick polyamide leaves. Overall, the TFC-PSf membranes (thick basal layer with thin polyamide leaves) and TFC-PEI membranes (thin basal layer with thick polyamide leaves) can attain fairly similar water permeabilities given that the overall resistance posed by the polyamide layer is the combination posed by the basal layer and polyamide leaves. Lastly, we would like to highlight that our proposed conceptual model is not definitive. For example, the conceptual model may not apply to systems involving other types of monomers such as piperazine (PIP), *p*-phenylenediamine (PPD) and terephthaloyl chloride (TPC) in the synthesis of RO membranes [1, 13, 50]. The varying properties of the monomers can induce different extents of cross-linking degree and free volume of the polyamide layer, both of which are critical factors that influence the water flux and salt rejection of the TFC membrane [1, 13].

4. Conclusions

This work unraveled the role of support membrane chemistry (under similar surface pore properties) on the desalination performance of TFC-RO membranes due to induced changes in nanoscale polyamide morphology. TEM analyses revealed the nanoscale differences in the polyamide layers, whereas XPS and FTIR analyses outlined the slight changes in polyamide cross-linking when the polyamide leaves became thicker. Several insights can be derived from this study:

(1) The hydrophilic PES supports (contact angle of ~50-60º) resulted in the formation of thin and smooth polyamide layers because of a slow and less extensive MPD diffusion into the organic phase. It is hypothesized that some of the polyamide layers sags into the pores of the support because of the affinity between the support and MPD.

(2) The hydrophobic PSf supports (contact angle of ~90º) resulted in the formation of a thick basal layer with thin polyamide leaves. The former arises from the fast MPD diffusion (both vertical and lateral) at the initial stage of IP whereas the latter is attributed to the broader IP reaction zone (such that MPD monomers were more spread out).

(3) As compared to the PSf supports, the moderately hydrophobic PEI supports (contact angle of ~70-80º) resulted in the formation of a thin basal layer underneath thick polyamide leaves. The former is likely to arise from a slower MPD diffusion at the initial stage of IP whereas the latter can be attributed to the localization of MPD reactants over a narrower IP reaction zone.

(4) The TFC-PES membranes showed much lower permeability as compared to TFC-PEI and TFC-PSf membranes, most likely because of the increased resistance for water diffusion over the selective layer.

Acknowledgements

This research grant was supported by the Singapore National Research Foundation under its Urban Solutions & Sustainability Program and administered by PUB, Singapore's National Water Agency (grant number: PUB-1801-0010). The Singapore Membrane Technology Center, Nanyang Environment and Water Research Institute, Nanyang Technological University is grateful for the funding support from the Economic Development Board of Singapore. We would like to thank Ms. Janelle Ng from NEWRI Analytics Cluster, Nanyang Technological University, Singapore, for helping with membrane characterization in TEM and XPS analyses.

References

[1] Y.J. Lim, K. Goh, M. Kurihara, R. Wang, Seawater desalination by reverse osmosis: Current development and future challenges in membrane fabrication–A review, J. Membr. Sci., 629 (2021) 119292.

[2] A.G. Fane, R. Wang, M.X. Hu, Synthetic membranes for water purification: status and future, Angew. Chem. Int. Ed., 54 (2015) 3368-3386.

[3] X. Dong, D. Lu, T.A. Harris, I.C. Escobar, Polymers and Solvents Used in Membrane Fabrication: A Review Focusing on Sustainable Membrane Development, Membranes, 11 (2021) 309.

[4] Z. Zhang, C. Yin, G. Yang, A. Xiao, X. Shi, W. Xing, Y. Wang, Stitching nanosheets of covalent organic frameworks to build aligned nanopores in nanofiltration membranes for precise ion separations, J. Membr. Sci., 618 (2021) 118754.

[5] K.P. Lee, G. Bargeman, R. de Rooij, A.J. Kemperman, N.E. Benes, Interfacial polymerization of cyanuric chloride and monomeric amines: pH resistant thin film composite polyamine nanofiltration membranes, J. Membr. Sci., 523 (2017) 487-496.

[6] J. Lee, R. Wang, T.-H. Bae, A comprehensive understanding of co-solvent effects on interfacial polymerization: Interaction with trimesoyl chloride, J. Membr. Sci., 583 (2019) 70-80.

[7] S.-J. Park, S.J. Kwon, H.-E. Kwon, M.G. Shin, S.-H. Park, H. Park, Y.-I. Park, S.-E. Nam, J.-H. Lee, Aromatic solvent-assisted interfacial polymerization to prepare high performance thin film composite reverse osmosis membranes based on hydrophilic supports, Polymer, 144 (2018) 159-167.

[8] D.H.N. Perera, Q. Song, H. Qiblawey, E. Sivaniah, Regulating the aqueous phase monomer balance for flux improvement in polyamide thin film composite membranes, J. Membr. Sci., 487 (2015) 74-82.

[9] Y. Zhao, G.S. Lai, Y. Wang, C. Li, R. Wang, Impact of pilot-scale PSF substrate surface and pore structural properties on tailoring seawater reverse osmosis membrane performance, J. Membr. Sci., 633 (2021) 119395.

[10] M. Kurihara, T. Sasaki, K. Nakatsuji, M. Kimura, M. Henmi, Low pressure SWRO membrane for desalination in the Mega-ton Water System, Desalination, 368 (2015) 135-139.

[11] T.E. Culp, B. Khara, K.P. Brickey, M. Geitner, T.J. Zimudzi, J.D. Wilbur, S.D. Jons, A. Roy, M. Paul, B. Ganapathysubramanian, Nanoscale control of internal inhomogeneity enhances water transport in desalination membranes, Science, 371 (2021) 72-75.

[12] A.K. Ghosh, E.M. Hoek, Impacts of support membrane structure and chemistry on polyamide–polysulfone interfacial composite membranes, J. Membr. Sci., 336 (2009) 140-148.
[13] Y. Zhao, Z. Zhang, L. Dai, H. Mao, S. Zhang, Enhanced both water flux and salt rejection of reverse osmosis membrane through combining isophthaloyl dichloride with biphenyl tetraacyl chloride as organic phase monomer for seawater desalination, J. Membr. Sci., 522 (2017) 175-182.
[14] K. Goh, H.E. Karahan, L. Wei, T.-H. Bae, A.G. Fane, R. Wang, Y. Chen, Carbon nanomaterials for advancing separation membranes: A strategic perspective, Carbon, 109 (2016) 694-710.
[15] H. Zheng, Z. Mou, K. Zhou, Incorporation of Core–Shell-Structured Zwitterionic Carbon Dots in Thin-Film Nanocomposite Membranes for Simultaneously Improved Perm-Selectivity and Antifouling Properties, ACS Applied Materials & Interfaces, 12 (2020) 53215-53229.
[16] C. Li, S. Li, J. Zhang, C. Yang, B. Su, L. Han, X. Gao, Emerging sandwich-like reverse osmosis membrane with interfacial assembled covalent organic frameworks interlayer for highly-efficient desalination, J. Membr. Sci., 604 (2020) 118065.
[17] Y.J. Lim, S.M. Lee, R. Wang, J. Lee, Emerging Materials to Prepare Mixed Matrix Membranes for Pollutant Removal in Water, Membranes, 11 (2021) 508.
[18] N. Akther, Y. Kawabata, S. Lim, T. Yoshioka, S. Phuntsho, H. Matsuyama, H.K. Shon, Effect of graphene oxide quantum dots on the interfacial polymerization of a thin-film nanocomposite forward osmosis membrane: An experimental and molecular dynamics study, J. Membr. Sci., 630 (2021) 119309.
[19] S. Chou, R. Wang, A.G. Fane, Robust and high performance hollow fiber membranes for energy harvesting from salinity gradients by pressure retarded osmosis, J. Membr. Sci., 448 (2013) 44-54.
[20] Y.J. Lim, J. Lee, T.-H. Bae, J. Torres, R. Wang, Feasibility and performance of a thin-film composite seawater reverse osmosis membrane fabricated on a highly porous microstructured support, J. Membr. Sci., (2020) 118407.
[21] J. Lee, R. Wang, T.-H. Bae, High-performance reverse osmosis membranes fabricated on highly porous microstructured supports, Desalination, 436 (2018) 48-55.
[22] M. Pagliero, A. Bottino, A. Comite, C. Costa, Novel hydrophobic PVDF membranes prepared by nonsolvent induced phase separation for membrane distillation, J. Membr. Sci., 596 (2020) 117575.

[23] Y.J. Lim, K. Goh, G.S. Lai, C.Y. Ng, J. Torres, R. Wang, Fast water transport through biomimetic reverse osmosis membranes embedded with peptide-attached (pR)-pillar [5] arenes water channels, J. Membr. Sci., 628 (2021) 119276.
[24] M. Shi, Z. Wang, S. Zhao, J. Wang, P. Zhang, X. Cao, A novel pathway for high performance RO membrane: preparing active layer with decreased thickness and enhanced compactness by incorporating tannic acid into the support, J. Membr. Sci., 555 (2018) 157-168.
[25] K. Goh, L. Setiawan, L. Wei, R. Si, A.G. Fane, R. Wang, Y. Chen, Graphene oxide as effective selective barriers on a hollow fiber membrane for water treatment process, J. Membr. Sci., 474 (2015) 244-253.
[26] X. Bao, W. Long, H. Liu, Q. She, Boron and salt ion transport in electrically assisted reverse osmosis, J. Membr. Sci., (2021) 119639.
[27] Y. Hai, J. Zhang, C. Shi, A. Zhou, C. Bian, W. Li, Thin film composite nanofiltration membrane prepared by the interfacial polymerization of 1, 2, 4, 5-benzene tetracarbonyl chloride on the mixed amines cross-linked poly (ether imide) support, J. Membr. Sci., 520 (2016) 19-28.
[28] M. Namvar-Mahboub, M. Pakizeh, Development of a novel thin film composite membrane by interfacial polymerization on polyetherimide/modified SiO2 support for organic solvent nanofiltration, Sep. Purif. Technol., 119 (2013) 35-45.
[29] U. Sathya, M. Nithya, Fabrication and characterisation of fine-tuned Polyetherimide (PEI)/WO3 composite ultrafiltration membranes for antifouling studies, Chem. Phys. Lett., 744 (2020) 137201.
[30] N. Misdan, W. Lau, A. Ismail, T. Matsuura, D. Rana, Study on the thin film composite poly (piperazine-amide) nanofiltration membrane: Impacts of physicochemical properties of substrate on interfacial polymerization formation, Desalination, 344 (2014) 198-205.
[31] Y. Li, S. Qi, M. Tian, W. Widjajanti, R. Wang, Fabrication of aquaporin-based biomimetic membrane for seawater desalination, Desalination, 467 (2019) 103-112.
[32] T.H. Lee, M.Y. Lee, H.D. Lee, J.S. Roh, H.W. Kim, H.B. Park, Highly porous carbon nanotube/polysulfone nanocomposite supports for high-flux polyamide reverse osmosis membranes, J. Membr. Sci., 539 (2017) 441-450.
[33] C.M. Hansen, Hansen solubility parameters: a user's handbook, CRC press, 2007.
[34] S. Mazinani, S. Darvishmanesh, A. Ehsanzadeh, B. Van der Bruggen, Phase separation analysis of Extem/solvent/non-solvent systems and relation with membrane morphology, J. Membr. Sci., 526 (2017) 301-314.

[35] L. Setiawan, L. Shi, W.B. Krantz, R. Wang, Explorations of delamination and irregular structure in poly (amide-imide)-polyethersulfone dual layer hollow fiber membranes, J. Membr. Sci., 423 (2012) 73-84.
[36] X. Dong, T.J. Jeong, E. Kline, L. Banks, E. Grulke, T. Harris, I.C. Escobar, Eco-friendly solvents and their mixture for the fabrication of polysulfone ultrafiltration membranes: An investigation of doctor blade and slot die casting methods, J. Membr. Sci., 614 (2020) 118510.
[37] L. Zhang, Z. Cui, M. Hu, Y. Mo, S. Li, B. He, J. Li, Preparation of PES/SPSf blend ultrafiltration membranes with high performance via H2O-induced gelation phase separation, J. Membr. Sci., 540 (2017) 136-145.
[38] Y. Li, R. Wang, S. Qi, C. Tang, Structural stability and mass transfer properties of pressure retarded osmosis (PRO) membrane under high operating pressures, J. Membr. Sci., 488 (2015) 143-153.
[39] S. Alibakhshi, M. Youssefi, S.S. Hosseini, A. Zadhoush, Significance of thermodynamics and rheological characteristics of dope solutions on the morphological evolution of polyethersulfone ultrafiltration membranes, Polymer Engineering & Science, 61 (2021) 742-753.
[40] L. Huang, J.R. McCutcheon, Impact of support layer pore size on performance of thin film composite membranes for forward osmosis, J. Membr. Sci., 483 (2015) 25-33.
[41] J. Xu, H. Yan, Y. Zhang, G. Pan, Y. Liu, The morphology of fully-aromatic polyamide separation layer and its relationship with separation performance of TFC membranes, J. Membr. Sci., 541 (2017) 174-188.
[42] S.-J. Park, W. Choi, S.-E. Nam, S. Hong, J.S. Lee, J.-H. Lee, Fabrication of polyamide thin film composite reverse osmosis membranes via support-free interfacial polymerization, J. Membr. Sci., 526 (2017) 52-59.
[43] Q. Zhang, Z. Zhang, L. Dai, H. Wang, S. Li, S. Zhang, Novel insights into the interplay between support and active layer in the thin film composite polyamide membranes, J. Membr. Sci., 537 (2017) 372-383.
[44] Z. Ali, Y. Al Sunbul, F. Pacheco, W. Ogieglo, Y. Wang, G. Genduso, I. Pinnau, Defect-free highly selective polyamide thin-film composite membranes for desalination and boron removal, J. Membr. Sci., 578 (2019) 85-94.
[45] L.E. Peng, Y. Jiang, L. Wen, H. Guo, Z. Yang, C.Y. Tang, Does interfacial vaporization of organic solvent affect the structure and separation properties of polyamide RO membranes?, J. Membr. Sci., 625 (2021) 119173.

723 [46] X. Li, Q. Li, W. Fang, R. Wang, W.B. Krantz, Effects of the support on the
724 characteristics and permselectivity of thin film composite membranes, J. Membr. Sci., 580
725 (2019) 12-23.
726 [47] J. Lee, F. Zhou, K. Baek, W. Kim, H. Su, K. Kim, R. Wang, T.-H. Bae, Use of rigid
727 cucurbit [6] uril mediating selective water transport as a potential remedy to improve the
728 permselectivity and durability of reverse osmosis membranes, J. Membr. Sci., (2020) 119017.
729 [48] J. Duan, Y. Pan, F. Pacheco, E. Litwiller, Z. Lai, I. Pinnau, High-performance polyamide
730 thin-film-nanocomposite reverse osmosis membranes containing hydrophobic zeolitic
731 imidazolate framework-8, J. Membr. Sci., 476 (2015) 303-310.
732 [49] W.D. Mulhearn, V.P. Oleshko, C.M. Stafford, Thickness-dependent permeance of
733 molecular layer-by-layer polyamide membranes, J. Membr. Sci., 618 (2021) 118637.
734 [50] Z. Ali, Y. Wang, W. Ogieglo, F. Pacheco, H. Vovusha, Y. Han, I. Pinnau, Gas
735 separation and water desalination performance of defect-free interfacially polymerized para-
736 linked polyamide thin-film composite membranes, J. Membr. Sci., 618 (2021) 118572.
737
738